Progress In Electromagnetics Research, PIER 60, 245–264, 2006

MIXED-POTENTIAL GREEN'S FUNCTION OF AN AXIALLY SYMMETRIC SHEET MAGNETIC CURRENT ON A CIRCULAR CYLINDRICAL METAL SURFACE

A. Y. Svezhentsev

The A.Ya. Usikov Institute of Radio Physics and Electronics
National Academy of Sciences of Ukraine
12, Akad. Proskury str., 61085, Kharkov, Ukraine

Abstract—An effective approach is suggested for calculating the Green's function of an axially symmetric sheet magnetic current placed on a circular cylindrical metal surface. Upon improving convergence of the available Fourier transform, it has been possible to explicitly develop the Green's function logarithmic singularity at the source. Also, the Green's function behavior at the branch point in the spectral domain has been considered, ending up with the singularity extraction in the space domain. It is shown that this branch point singularity (pole) corresponds to the cylindrical quasi-TEM mode of the cylinder exterior. Finally, the rest of the Green's function is effectively numerically calculated.

1. INTRODUCTION

The Green's function problem of an axially symmetric sheet magnetic current placed on a circular metal cylinder is an area of interest in conformal antenna theory [1, 2]. In particular, the conformal antenna can radiate via the aperture excitation, including an axially symmetric aperture on a cylindrical surface. The aperture, in turn, can be stimulated, for one, by a wave travelling in the cylinder interior. In this case, the equivalence principle [3] allows the aperture modeling as two sheets of oppositely directed magnetic currents placed in the aperture proximity on both sides of it [4]. The integral equation of the magnetic current on the aperture surface is formulated, and the space Green's function for the sheet magnetic current plays the key part there. The solution strategy implies the method of moments for solving the integral equation in the space domain.

The excitation of a circular metal cylinder by external currents is a classical problem, not new in the literature. In particular, the general problem solution upon inverse Fourier transform (IFT) in cylindrical coordinates is presented in [5]. Although the solution from [5] is numerically available for the external current in any appearance, the integral equation of the aperture radiation problem cannot be furnished in the considered problem when the aperture is accommodated on a cylindrical surface. The trouble is that the Green's function singularity at the source has not been developed yet.

The novelty of this paper is in that the source singularity of the spatial Greens function for an axially symmetric sheet magnetic current placed on the surface of a circular metal cylinder has been obtained in an explicit form. This has been reached by the extraction of the spectral Greens function asymptote in the spectral domain and the addition of its spatial-domain equivalent evaluated analytically. In addition, the branch point contribution to the spatial Greens function has been developed in a sufficiently explicit form. On this basis an effective algorithm of Green's function computation will be available wherever in the space domain, including the source region. Opposed to [5] with the IFT developed in χ, terms (χ is the transverse wave number), the IFT will be built in h terms (h is the longitudinal propagation constant). This strategy has been tried in [6] for constructing the Green's function of an electric current sheet on a dielectric coated metal cylinder.

2. PROBLEM FORMULATION

In Fig. 1, a circular metal cylinder of radius r_1 carries a sheet of axially symmetric magnetic current $\boldsymbol{J}^m(r_1, z)$ having z and φ components and distributed over a bounded surface S'. It is required to express the magnetic field components via the magnetic currents and find the Green's function.

Initially, let us suppose that the sheet of axially symmetric magnetic current is placed over the metal cylinder on the surface with $r = r_0 > r_1$. We link to the two regions $r_1 < r < r_0$ and $r > r_0$, with the corresponding affiliations designated by indices $p = 0$ and 1, respectively. Time dependence $e^{i\omega t}$ is assumed and suppressed. The z-components of the magnetic field in h-IFT terms [5] are

$$\{E_z^p(r,z), H_z^p(r,z)\} = \frac{1}{2\pi} \int\limits_{h=-\infty}^{\infty} \{e_z^p(r,h), h_z^p(r,h)\}\, e^{-ihz} dh, \quad (1)$$

where i is the imaginary unit and h is the propagation constant.

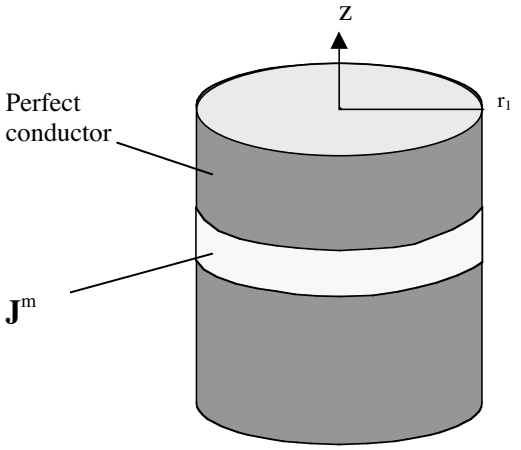

Figure 1. The excitation of the metal cylinder exterior by an axially symmetric sheet of surface magnetic current $\boldsymbol{J}^m$.

Expression (1) has the appearance of infinite spectrum of z-modulated cylindrical waves travelling in the radial direction.

In each region $p = 0, 1$, the field spectral components are sought as a solution of the one-dimensional Helmholtz equation

$$\left(\Delta + \tilde{k}^2\right) \{e_z^p(r,h), h_z^p(r,h)\} = 0. \tag{2}$$

Here Δ is the one-dimensional Laplace operator in variable r (the consideration is axially symmetric), $e_z^p(r,h)$ and $h_z^p(r,h)$ are the spectral components of the electric and magnetic fields, $\tilde{k}^2 = k_0^2 - h^2$, $k_0^2 = \omega^2 \cdot \varepsilon_0 \cdot \mu_0$ and $k_0 = 2\pi/\lambda_0$, where λ_0 is the free-space wavelength and ε_0, μ_0, are the absolute permittivity and permeability of a vacuum.

After satisfying the boundary condition on the metal conductor surface, one has the solution of (2) in the form

$$\{e_z^p(r,h), h_z^p(r,h)\} = \left\{B_p \gamma_p(r,h), \overline{B}_p \overline{\gamma}_p(r,h)\right\}, \tag{3}$$

with

$$\gamma_0(r,h) = \overline{\gamma}_0(r,h) = \frac{H_0^{(2)}(\tilde{k}r)}{H_0^{(2)}(\tilde{k}r_0)};$$

$$\{\gamma_1(r,h), \overline{\gamma}(r,h)\} = \frac{J_0(\tilde{k}r)}{J_0(\tilde{k}r_1)} + \left\{\Gamma_1 \frac{H_0^{(2)}(\tilde{k}r)}{H_0^{(2)}(\tilde{k}r_1)}, \overline{\Gamma}_1 \frac{H_0^{(2)}(\tilde{k}r)}{H_0^{(2)}(\tilde{k}r_1)}\right\};$$

$$\Gamma_1 = -\frac{J_0(\overline{x}_1)}{J_0(x_1)}\frac{H_0^{(2)}(x_1)}{H_0^{(2)}(\overline{x}_1)}; \quad \overline{\Gamma}_1 = -\frac{J_0'(\overline{x}_1)}{J_0(x_1)}\frac{H_0^{(2)}(x_1)}{H_0^{'(2)}(\overline{x}_1)}; \tag{4}$$

$$x_1^2 = (k_0 r_0)^2\{1-\overline{h}^2\}; \quad \overline{x}_1^2 = (k_0 r_1)^2\{1-\overline{h}^2\}; \quad \overline{h} = h/k_0,$$

where B_p, $\overline{B}_p$ are the unknown coefficients, $\overline{h}$ is the normalized propagation constant, and $J_0(x)$ and $H_0^{(2)}(x)$ are the zero-order Bessel and Hankel functions, respectively. The coefficients B_p, $\overline{B}_p$ come from satisfying the boundary condition on the magnetic current interface $r = r_0$

$$e_\varphi^0(r_0,h) - e_\varphi^1(r_0,h) = -j_z^m(h), \quad h_z^0(r_0,h) - h_z^1(r_0,h) = 0, \tag{5a}$$

$$e_z^0(r_0,h) - e_z^1(r_0,h) = -j_\varphi^m(h), \quad h_\varphi^0(r_0,h) - h_\varphi^1(r_0,h) = 0, \tag{5b}$$

where $j_s^m(h)$ is the direct Fourier transform of surface currents $J_s^m(r_1,z)$; subscript s stands for either z or φ. In (5a) and (5b), the transverse components are expressed via the longitudinal components in the well-known manner [5]. As the axial symmetry case goes with polarization splitting, the consideration falls into the two independent problems for the H-waves (H_z, H_r, E_φ) (5a) and the E-waves (E_z, E_r, H_φ) (5b) produced, respectively, by the z- and φ-components of the magnetic current. Coefficients B_p, $\overline{B}_p$ are provided by Appendix A.

From now on, the sheet magnetic current will be placed on the metal cylinder surface (some relevant transformations can be found in Appendix A). Hence $r_0 = r_1$, and the spectral components of the magnetic field on the interface $r = r_1$ are (in the following, the superscript of the spectral field will be omitted)

$$h_z(r_1,h) = \chi_z^m(r_1,h)\cdot j_z^m(h) \tag{6}$$

$$h_\varphi(r_1,h) = \chi_\varphi^m(r_1,h)\cdot j_\varphi^m(h) \tag{7}$$

For spectral functions $\chi_s^m(r_1,h)$, see Appendix A.

The further step should be the transformation of (6) and (7) for the space domain. To improve the Green's function convergence in the space domain, (6) is expressed in terms of so-called mixed potentials [6] as follows

$$h_z(r_1,h) = \chi_z^m(r_1,h)j_z^m(h) = g_z^{mJ}(r_1,h)j_z^m(h) + ihg^{m\sigma}(r_1,h)ihj_z^m(h). \tag{8}$$

For spectral functions $g_s^{m(J,\sigma)}$, see Appendix A. Formula (8) is the definition of changing from the standard formulation to that in the

mixed-potential form; superscripts J and σ stand for current and charge, respectively. Notice that in the considered axially symmetric case, (7) need not be changed as just shown. Transforming (6) and (7) from the spectral to the space domain yields the magnetic field components in current terms with the use of Green's functions as follows

$$H_z(r_1,z) = \int_0^L J_z^m(z')G_z^{mJ}(r_1,z-z')dz' + \frac{d}{dz}\int_0^L \nabla_t' \boldsymbol{J}^m(z')G^{m\sigma}(r_1,z-z')dz' \tag{9}$$

$$H_\varphi(r_1,z) = \int_0^L J_z^m(z')G_\varphi^{mJ}(r_1,z-z')dz', \tag{10}$$

where L is the linear size of the axially symmetric sheet current in the z-direction, $\nabla_t' = \boldsymbol{z}_0\frac{\partial}{\partial z'}$, and the Green's function is

$$G_s^{m(J,\sigma)}(r_1,z-z') = \frac{1}{2\pi}\int_{h=-\infty}^{\infty} g_s^{m(J,\sigma)}(r_1,h)e^{-ih(z-z')}dh. \tag{11}$$

The second term is missing from (7), (10) because $\frac{\partial}{\partial\varphi}=0$ in the axially symmetric case. The integration in (11) proceeds along the real axis of propagation constant h (Fig. 2).

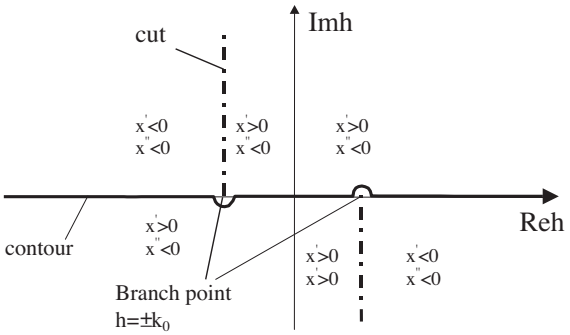

Figure 2. The basic sheet of the Riemann surface; x' and x' stand for the real and the imaginary parts of $x = kr_1\sqrt{1-\overline{h}^2}$, respectively.

Now that (9), (10) have been obtained, the key problem is the evaluation of Green's function (11). The straightforward calculation is not possible because of the singular behavior of the spectral function. The primary trouble is a slow decrease of the spectral Green's function in parameter h. Furthermore, the integral of (11) diverges as the observation point approaches the source. The second trouble is the branch point singularity of the spectral Green's functions. In the further paragraphs, some ways of effective calculation of (11) will be discussed.

3. ASYMPTOTIC BEHAVIOR OF SPECTRAL GREEN'S FUNCTIONS AT A LARGE $\overline{h}$. GREEN'S FUNCTION SINGULARITY AT THE SOURCE

Examine the asymptotic behavior of the spectral Green's functions as $\overline{h} \to \infty$. From (4) it follows that the arguments of the cylindrical functions are purely imaginary when $\overline{h} \to \infty$. Then the cylindrical functions change into the modified cylindrical functions (see Appendix B) approximated in the large argument case to the leading term (B4).

Insert (B4) into (B2) to get spectral Green's functions $g_s^{m(J,\sigma)}(r_1, h)$ in the asymptotic representation

$$g_s^{AS,m(J,\sigma)}(r_1, \overline{h}) = \frac{A_s^{J,\sigma} f(\overline{h})}{k_0 r_1 \overline{h}}, \tag{12}$$

$$A_z^J = A_\varphi^J = 1/w_0; \quad A_z^\sigma = 1/(k_0^2 w_0); \quad f(\overline{h}) = 1 - e^{-k_0 t \overline{h}},$$

where $w_0 = \sqrt{\mu_0/\varepsilon_0}$ is the wave resistance of the free space.

Notice the introduction of complementary function $f(\overline{h})$ into (12) to compensate the singular behavior at $\overline{h} = 0$. However arbitrarily valued, quantity $k_0 t$ is necessarily positive to provide the decrease as $\overline{h}$ grows. The appearance of (12) reveals a slow decay of the spectral Green's function, which causes, as will be seen later, the source singularity in the space domain. The spectral Green's functions $g_s^{mJ}(r_1, h)$ and their asymptotes $g_s^{AS,mJ}(r_1, h)$ are viewed in Fig. 3.

Formulae (A5) show that the spectral Green's functions are even functions of h. This makes us free to take the integrals of (11) over $(0, \infty)$. So

$$G_s^{m(J,\sigma)}(r_1, z - z') = \frac{1}{\pi} \int_0^\infty g_s^{m(J,\sigma)}(r_1, h) \cos[h(z - z')] dh. \tag{13}$$

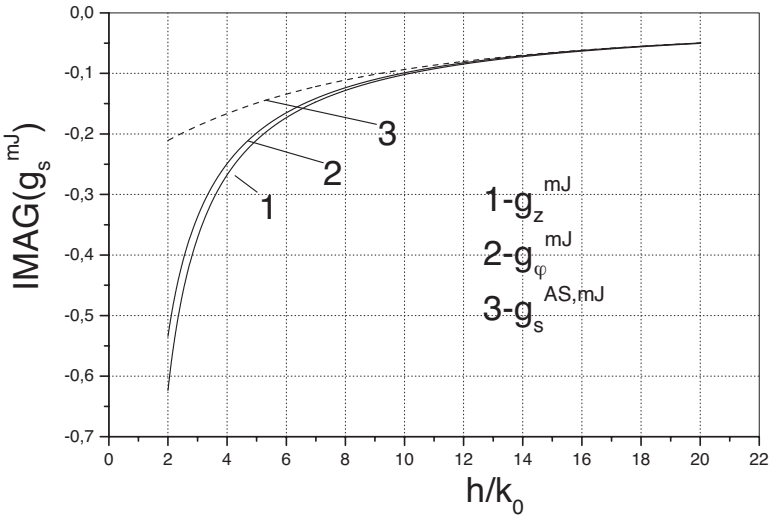

Figure 3. The spectral Green's functions $g_s^{mJ}(r_1, h)$ and the spectral asymptote $g_s^{AS,mJ}(r_1, h)$ versus normalized propagation constant $\overline{h} = h/k_0$ in the region $\overline{h} > 2$ at $f = 3.3\,\mathrm{GHz}$ and $r_1 = 0.05\,\mathrm{m}$.

Rearrange the integrand in (13) by adding and subtracting the asymptotic behavior of spectral Green's function (12). In turn, the IFT of the spectral asymptote

$$G_s^{SING,m(J,\sigma)}(r_1, z - z') = \frac{1}{\pi} \int_0^\infty g_s^{AS,m(J,\sigma)}(r_1, h) \cos[h(z - z')] dh \quad (14)$$

is calculated by the formula [9]

$$\int_0^\infty \frac{(1 - e^{-d\overline{h}})}{\overline{h}} \cos(b\overline{h}) d\overline{h} = \frac{1}{2} \ln\left(\frac{b^2 + d^2}{b^2}\right). \quad (15)$$

The final explicit representation of the singular part of the Green's function in the space domain is

$$G_s^{SING,m(J,\sigma)}(r_1, z - z') = -\frac{ik_0 A_{z,\varphi}^{J,\sigma}}{4\pi} \ln \frac{[k_0^2(z - z')^2 + (k_0 t)^2]}{[k_0^2(z - z')^2]}. \quad (16)$$

According to (16), the Green's function has a logarithmic singularity at the source.

4. BRANCH POINT BEHAVIOR OF SPECTRAL GREEN'S FUNCTIONS $g_{\varphi}^{m,J}$ AND $g_{z}^{m,J}$

Recall that the Fourier integral in (13) is taken along the real axis of propagation constant h (see Fig. 2). To be more specific, the area of the analytic continuation of the spectral Green's function is the infinite-sheeted Rieamann surface of the function $\ln[(h-k_0)(h+k_0)]$. The points $h=\pm k_0$are branch points. The integral in (13) is taken along the real axis of the Riemann basis sheet defined by the conditions $\mathrm{Im}\sqrt{k_0^2-h^2}<0$ for $|h|>k_0$ and $-\pi/2<Arg\sqrt{k_0^2-h^2}<\pi/2$. To develop the square root branches, the cuts are made from the branch points to the infinity, as shown in Fig. 2. The integration contour bypasses the branch points so as to satisfy the radiation condition, or what is the same, the limiting absorption principle [7].

Consider the branch point behavior of the spectral Green's functions. Owing to the small-argument asymptotic representation of the Hankel function with its derivative ($x<1$ or $z<1$) [8], functions $g_s^{m(J,\sigma)}$ given by (A5) can be approximated in the branch point vicinity $\overline{h}<1$ and $\overline{h}>1$ as follows

$$g_z^{mJ} = k_0^2 g_z^{m\sigma} = -\frac{\pi k_0 r_0}{2}\left(1+x^2\ln\frac{\gamma x}{2}\right)+i\left[-\frac{k_0 r_0 \pi^2}{8}x^2+\ln\frac{\gamma x}{2}\right] \quad \text{for } \overline{h}<1, \tag{17}$$

$$g_z^{mJ} = k_0^2 g_z^{m\sigma} = i\ln\frac{\gamma z}{2} \quad \text{for } \overline{h}>1, \tag{18}$$

$$g_{\varphi}^{mJ} = -\frac{(2/\pi)k_0 r_1}{x[1+(4/\pi^2)\ln^2(\gamma x/2)]}-i\frac{(4/\pi^2)k_0 r_1\ln(\gamma x/2)}{x^2[1+(4/\pi^2)\ln^2(\gamma x/2)]} \quad \text{for } \overline{h}<1, \tag{19}$$

$$g_{\varphi}^{mJ} = i\frac{k_0 r_1}{z^2\ln(\gamma z/2)} \quad \text{for } \overline{h}>1, \tag{20}$$

where

$$\gamma=1.781072, \quad x\approx 2k_0 r_1\sqrt{1-\overline{h}}, \text{ and } z\approx 2k_0 r_1\sqrt{\overline{h}-1}. \tag{21}$$

Note that the spectral Green's functions demonstrate a singular behavior near the branch point. From (17)–(18) it follows that the real part of $g_z^{m(J,\sigma)}(h)$ is a discontinuous function having different limiting values, zero and a constant, as $\overline{h}\to 1$ from the right and from the left, respectively. The branch point behavior of the rigorous and

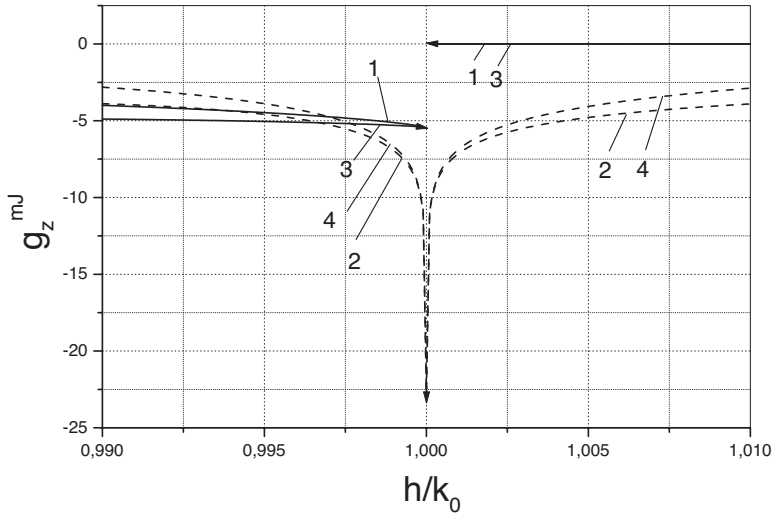

Figure 4. The real (solid line) and imaginary (dashed line) parts of the spectral Green's function $g_z^{mJ}(r_1, h)$ versus normalized propagation constant $\overline{h} = h/k_0$ in the branch point vicinity at $f = 3.3\,\mathrm{GHz}$ and $r_1 = 0.05\,\mathrm{m}$. Curves 1 and 2 correspond to the rigorous calculation, 3 and 4 come from approximate formulas (17)–(18).

the approximately calculated by (17)–(18) spectral Green's function $g_z^{m(J,\sigma)}(h)$ is viewed in Fig. 4. According to (17)–(18), the imaginary part $g_z^{m(J,\sigma)}(h)$ of has a logarithmic singularity at the branch point. Even though the singularity is integrable, it is good to analytically evaluate the integral of the imaginary part of function $g_z^{(mJ)}$ using approximation (17)–(18).

Thus, the singular behavior of $g_z^{m(J,\sigma)}(h)$ in the branch point vicinity is accounted for both the cylindrical functions such as the logarithm-carrying zero-order Hankel function and the mixed potential scheme causing the singular factor $1/x^2$ (see (A4)–(A5)).

Consider the branch point behavior of function g_φ^{mJ} shown in Fig. 5. There the rigorous data are compared with the approximate calculations by (19)–(20). According to (19)–(20), both the real and the imaginary parts of $g_\varphi^{mJ}(h)$ are discontinuous functions with a singularity at the branch point: the real part of $g_\varphi^{mJ}(h)$ possesses an integrable singularity, while the imaginary part of $g_\varphi^{mJ}(h)$ has a nonintegrable singularity $O(1/x^2 \ln(x))$. Notice that in this case the

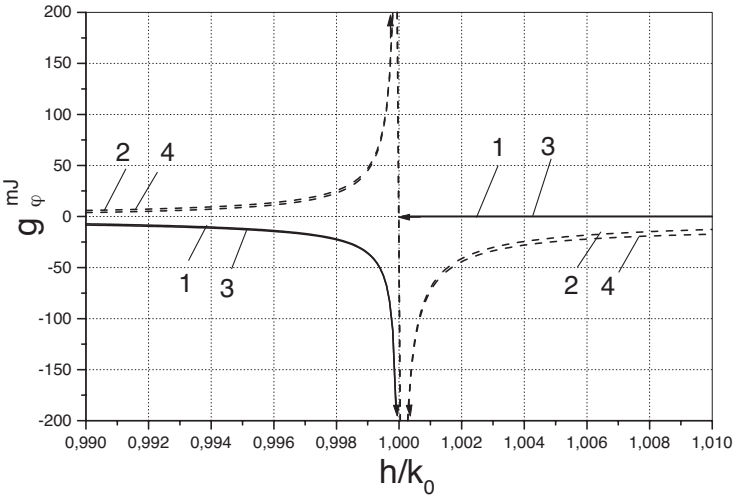

Figure 5. The spectral Green's function $g_{\varphi}^{mJ}(r_1, h)$ versus normalized propagation constant $\overline{h} = h/k_0$ in the branch point vicinity at $f = 3.3\,\text{GHz}$ and $r_1 = 0.05\,\text{m}$. The solid line is for the real part of the spectral Green's function, the dashed line is for the imaginary part. Curves 1 and 2 correspond to the rigorous calculation, curves 3 and 4 come from approximate formulas (19)–(20).

mixed potential scheme has not been introduced with any singularity added.

Despite the fact of nonintegrable singularity, integral (13) of function g_{φ}^{mJ} exists in the sense of principal value and can be evaluated. Some important comments on improper integrals appearing in EM theory can be found in [11].

5. GREEN'S FUNCTION EVALUATION

Now the space Green's function can be written as a sum of the singular and numerical parts

$$G_s^{m(J,\sigma)}(r_1, z - z') = G_s^{SING,m(J,\sigma)}(r_1, z - z') + G_s^{NUM,m(J,\sigma)}(r_1, z - z'). \tag{22}$$

In the numerical part, the Δ-vicinity of the branch point is developed and treated as follows

$$G_s^{NUM,m(J,\sigma)}(r_1, z - z') = G_s^{BRA,(mJ)}(r_1, z - z') + G1_s^{NUM,m(J,\sigma)}(r_1, z - z') \tag{23}$$

$$G1_s^{NUM,m(J,\sigma)}(r_1, z-z') = \frac{k_0}{\pi}\int_0^{1-\Delta} g1_s^{m(J,\sigma)}(r_1,\overline{h})\cos[\overline{h}k_0(z-z')]d\overline{h} + \frac{k_0}{\pi}\int_{1+\Delta}^{\infty} g1_s^{m,(J,\sigma)}(r_1,\overline{h})\cos[\overline{h}k_0(z-z')]d\overline{h} - \frac{k_0}{\pi}\int_{1-\Delta}^{1+\Delta} g_s^{AS,m(J,\sigma)}(r_1,\overline{h})\cos[\overline{h}k_0(z-z')]d\overline{h} \quad (24)$$

$$G_s^{BRA,(mJ,\sigma)}(r_1, z-z') = \frac{k_0}{\pi}\int_{1-\Delta}^{1+\Delta} g_s^{m(J,\sigma)}(r_1,\overline{h})\cos[\overline{h}k_0(z-z')]d\overline{h} \quad (25)$$

$$g1_s^{m(J,\sigma)}(r_1,\overline{h}) = g_s^{m(J,\sigma)}(r_1,\overline{h}) - g_s^{AS,m(J,\sigma)}(r_1,\overline{h}) \quad (26)$$

For the further details of the $G_s^{BRA,(mJ,\sigma)}$ evaluation, see Appendix C.

With the spectral Green's function decrease as $O(h^{-1})$ in view of (12), the finding of Green's function (13) reduces to the evaluation of IFT (24)–(25) of a function decreasing at least as $O(h^{-2})$, which is good enough to provide the numerical calculations. Notice that of the three spectral Green's functions of (11), only two need be calculated because $g_z^{m,J}(r_0,h) = k_0^2 g_z^{m,\sigma}(r_0,h)$.

The numerically obtained space Green's functions are viewed in Figs. 6a (G_z^{mJ}) and 6b (G_φ^{mJ}). The Green's functions $G_s^{NUM,mJ}$ (not plotted separately) run their peaks at the source point remaining finite. To better visualize the physics of the curves of Fig. 6 and compare them with the results of [5], the currents are put in the circular (ring-shaped) dipole form

$$J_\varphi^{mJ}(r_1,z') = I_{0\varphi}^m\delta(z'-0), \quad (27)$$

$$J_z^{mJ}(r_1,z') = I_{0z}^m\delta(z'-0). \quad (28)$$

This assumption simplifies the relationship between the magnetic field components and the Green's functions in (9) and (10). Namely, as shown in Appendix D,

$$H_\varphi(r_1,z) = 2\pi I_{0\varphi}^m r_1 G_\varphi^{mJ}(r_1,z-0), \quad (29)$$

$$H_z(r_1,z) = 2\pi r_1 I_{0z}^m \Phi(z-z')|_{z'=0}, \quad (30)$$

where function $\Phi(z-z')$ comes from (D5). Also, $J_z^e = H_\varphi$ and $J_\varphi^e = -H_z$ at the perfectly conducting surface.

Analysis of the curves of Fig. 6 and the results from Appendix D suggest the following conclusion. First, as one would expect, the Green's functions oscillate with a period equal to the free space wavelength, which means dealing with space waves whose phase velocities are equal to the speed of light in free space. Second, the amplitude of the space wave related to the J_z^e component of the electric current decreases much slower than the J_φ^e-related amplitude does. The reason is that the φth magnetic current excites a weakly radiating cylindrical quasi-TEM wave [5]. It is this wave that causes the singular behavior of the spectral Green's function. And as this wave magnetic field is purely transverse, no other electric current but longitudinal appears on the cylinder surface.

The problem of metal cylinder excitation by a circular dipole as that of (27) has been treated in [5], ending up with the current component expression

$$J_z^e = H_\varphi = \frac{I_0^m \omega \varepsilon_0}{2\pi} \int\limits_{\chi=-\infty}^{\infty} \frac{e^{\pm\sqrt{\chi^2-k^2}z}}{\sqrt{\chi^2-k^2}} \frac{H_0^{(2)'}(\chi r_1)}{H_0^{(2)}(\chi r_1)} d\chi. \tag{31}$$

In (31), the χ-IFT is seen as an infinite spectrum of plane cylindrical waves propagating along the z-axis in both directions from the source. Except for the source region, the numerical analysis of (31) was made [5], the current component J_z^e on the cylinder surface was plotted for different values of $k_0 r_1$ parameter. The J_z^e results obtained in the present paper fully agree with that from [5]. In support, the amplitude and the phase of the electric current component J_z^e normalized, as in [5], to $2I_{0\varphi}^m/(\pi^2 r_1)$ and calculated for four values of $k_0 r_1$ are plotted in Fig. 7a versus $k_0(z-z')$ parameter.

Fig. 7a evidences that the larger is $k_0 r_1$, the sharper is the decay of the electric current amplitude away from the origin. In physical terms, an electrically small cylinder supports the cylindrical quasi-TEM mode with less attenuation than an electrically large cylinder does. Also, in Fig. 7a, results obtained in [5] using formula (31) are plotted with circles.

According to Fig. 7b, the wave phase velocity equals the speed of light. Namely,

$$v_{\Phi a3} = ck_0 \left[\frac{d\psi}{dz}\right]^{-1} = c. \tag{32}$$

The curves of Figs. 7a,b coincide, within the graphical accuracy, with the results from [5].

It is important that the χ-expansion integrand in (31) is not even, whereas the h-expansion in (13) is. Attempts at developing

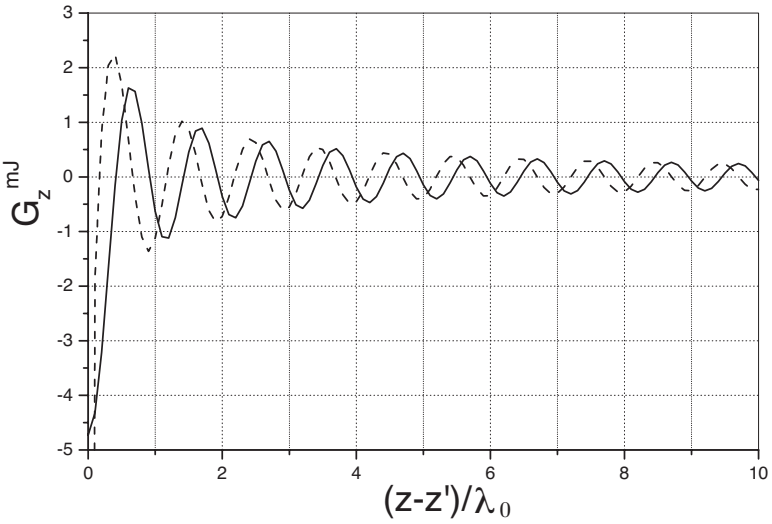

(a)

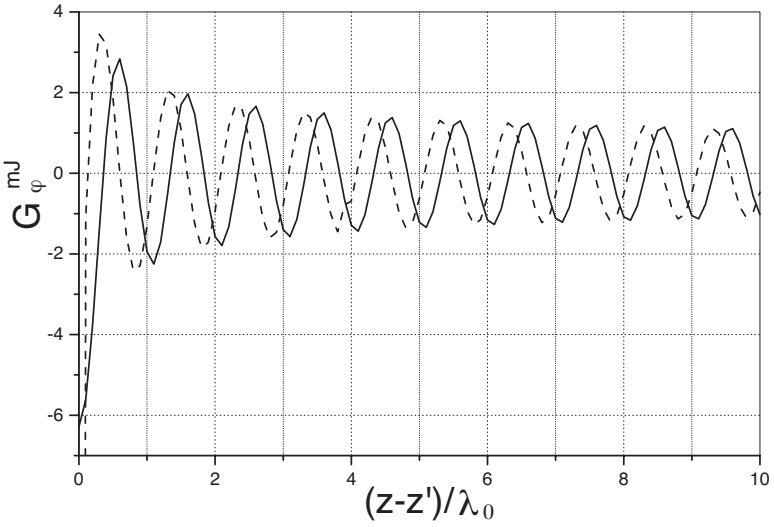

(b)

Figure 6. Green's function $G_s^{mJ}(r_1, z - z')$ versus the wavelength-normalized source distance $(z-z')/\lambda_0$ at $f = 3.3\,\mathrm{GHz}$ and $r_1 = 0.05\,\mathrm{m}$: (a) for $G_z^{mJ}(r_1, z - z')$ and (b) for $G_\varphi^{mJ}(r_1, z - z')$. In both figures, the solid line shows the real part of the Green's function, the dashed line is for the imaginary part.

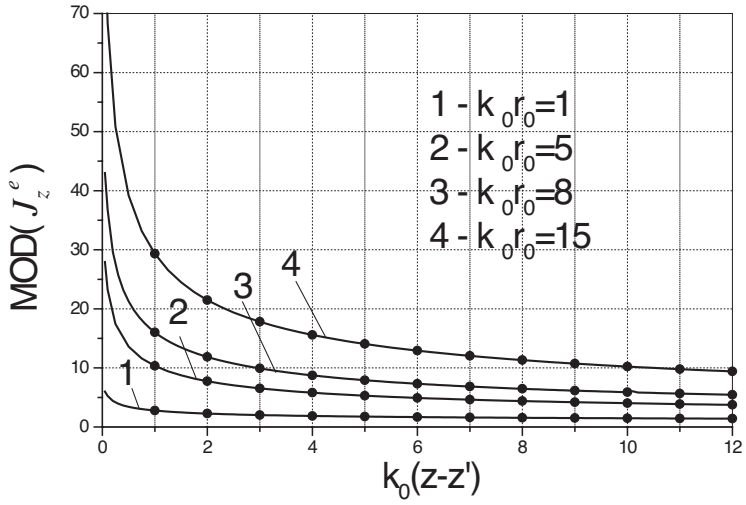

(a)

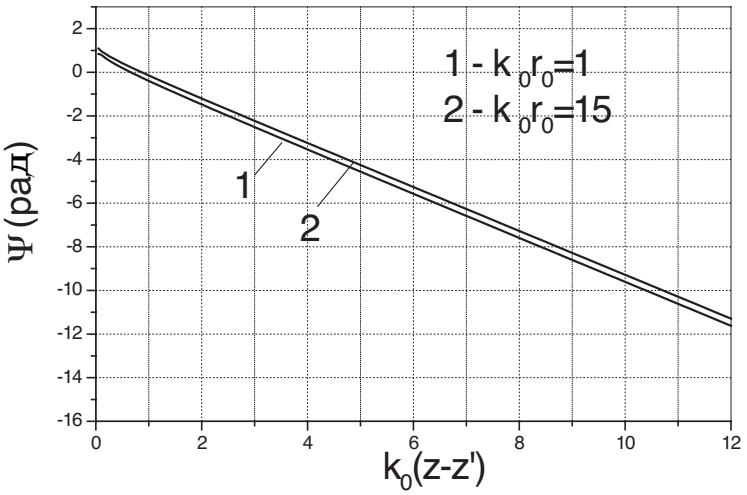

(b)

Figure 7. The amplitude (a) and the phase (b) of the electric current component J_z^e (normalized to $2I_{0\varphi}^m/\pi^2 r_1$) on the metal cylinder versus parameter $k_0(z-z')$; current phase Ψ is in radians.

the singularity of (31) by means of the asymptote explicit inversion yield the integral unsolvable in elementary functions. Therefore the h-expansion taken in the present study suits better for the development of Green's function singularity at the source.

6. CONCLUSION

Thus, an effective approach has been presented for calculating the Green's function of an axially symmetric sheet magnetic current placed on a circular metal cylinder. In essence, the method reduces to the extraction of the asymptotic behavior of the Green's function in the spectral domain with the addition of this function IFT in the space domain. As a result, the Green's function appears to consist of two terms. The first explicitly describes the field singularity at the source, while the second is effectively computer calculated. Also, the spectral Green's function specific features in the branch point vicinity have been traced. Some ways of the integration of the singular behavior of the spectral Green's functions have been shown. This singular behavior is due to the quasi-TEM wave, which propagates along the cylinder. The obtained Green's function is good enough to solve the radiation problem of an aperture accommodated on a cylindrical surface. The problem extension to the case of non-symmetric sheet magnetic current will be the topic of a separate paper. There the singularity development will be reported for spatial Green's function of sheet magnetic current of an arbitrary (non-symmetric) distribution.

ACKNOWLEDGMENT

The author would like to thank V. Kryzhanovsky and V. Volsky for their helpful comments made in the present paper discussions.

APPENDIX A. SPECTRAL GREEN'S FUNCTIONS

Coefficients B_p, $\overline{B}_p$ are expressed as

$$\begin{aligned} B_0 &= \frac{iF_0}{\Delta_0^E} j_\varphi^m(h), \quad \overline{B}_0 = \chi_z^m(r_0,h) j_z^m(h), \\ B_1 &= \frac{B_0 - j_\varphi^m(h)}{\gamma_1(r_0)}, \quad \overline{B}_1 = \frac{\overline{B}_0 + j_\varphi^m(h)}{\overline{\gamma}_1(r_0)}. \end{aligned} \tag{A1}$$

where

$$\chi_z^m(r_0,h) = -\frac{1}{\Delta_0^H w_0 k_0 r_0}, \quad \Delta_0^E = -i[\Phi_0 - F_0], \quad \Delta_0^H = i[\Phi_0 - \overline{F}_0],$$

$$\Phi_0 = \frac{\gamma_0'(r_0)}{x_1\gamma_0(r_0)}, \quad F_0 = \frac{\gamma_1'(r_0)}{x_1\gamma_1(r_0)}, \quad \overline{F}_0 = \frac{\overline{\gamma}_1'(r_0)}{x_1\overline{\gamma}_1(r_0)}.$$

In view of (A1), the spectral components of the tangential magnetic fields $h_z^0(r,h)$ and $h_\varphi^0(r,h)$ can be written as

$$h_z^0(r_0,h) = \chi_z^m(r_0,h)\cdot j_z^m(h) \tag{A2}$$

$$h_\varphi^0(r_0,h) = \chi_\varphi^m(r_0,h)\cdot j_\varphi^m(h) \tag{A3}$$

where

$$\chi_\varphi^m(r_0,h) = \frac{k_0 r_0}{w_0}\Phi_0 F_0 \frac{1}{\Delta_0^E}$$

Now the magnetic current is attached to the metal surface, $r_0 = r_1$ and the spectral Green's functions $\chi_s^m(r_1,h)$ become

$$\chi_z^m(r_1,h) = -\frac{i}{w_0}\frac{H_0^{(2)}(x)}{H_0^{(2)'}(x)}\frac{x}{k_0 r_1}, \quad \chi_\varphi^m(r_1,h) = -\frac{k_0 r_0}{w_0}\frac{H_0^{(2)'}}{H_0^{(2)}(x)}. \tag{A4}$$

Then the mixed-potential spectral Green's functions $g_s^{m(J,\sigma)}(r_1,h)$ are found in accordance with (8) in the form

$$g_z^{m,J}(r_1,h) = k_0^2 g^{m\sigma}(r_1,h) = -\frac{i}{w_0}\frac{H_0^{(2)}(x)}{H_0^{(2)'}(x)}\frac{k_0 r_1}{x}, \;\; g_\varphi^{m,J}(r_1,h) = \chi_\varphi^m(r_1,h), \tag{A5}$$

where $x = (k_0 r_1)\sqrt{1-\overline{h}^2}$.

APPENDIX B. ASYMPTOTIC REPRESENTATION OF SPECTRAL GREEN'S FUNCTIONS

When $\overline{h} > 1$, argument x of the cylindrical functions is purely imaginary

$$x = -iz, \qquad z = k_0 r_1\sqrt{\overline{h}^2 - 1}. \tag{B1}$$

Then functions $H_0^{(2)}(x)$ and $H_1^{(2)}(x)$ are expressible via the modified Macdonald functions $K_0(z)$ and $K_1(z)$, respectively, and the spectral Green's functions $g_s^{m(J,\sigma)}(r_1,h)$ (A5) are rewritten as

$$g_z^{m,J}(r_1,h) = -\frac{i}{w_0}\frac{K_0(z)}{K_1(z)}\frac{k_0 r_1}{z}, \quad g_\varphi^{mJ}(r_1,h) = -\frac{ik_0 r_1}{w_0}\frac{K_1}{zK_0(z)}. \tag{B2}$$

When $\overline{h} \to \infty$, argument z of the cylindrical function is approximately [8]

$$z \approx \overline{z} = k_0 r_1 \overline{h}, \tag{B3}$$

and the Macdonald functions can be approximated as follows

$$K_0(\overline{z}) \approx \sqrt{\frac{\pi}{2\overline{z}}} e^{-\overline{z}} \left\{1 - \frac{1}{8\overline{z}}\right\}; \quad K_1(\overline{z}) \approx \sqrt{\frac{\pi}{2\overline{z}}} e^{-\overline{z}} \left\{1 + \frac{3}{8\overline{z}}\right\}. \tag{B4}$$

Inserting the expansion leading terms (B4) into (B2) yields the asymptotic representation of Green's functions (12).

APPENDIX C. CALCULATION OF $G_s^{BRA}(r_1, z - z')$

First consider function $G_\varphi^{BRA,(mJ)}(r_1, z - z')$ in the form

$$G_\varphi^{BRA,(mJ)}(r_1, z - z') = \frac{k_0}{\pi} \int\limits_{1-\Delta}^{1+\Delta} g_\varphi^{mJ}(r_1, \overline{h}) \cos\left[\overline{h} k_0 (z - z')\right] d\overline{h}. \tag{C1}$$

To calculate (C1), take some approximations. Namely, since $\Delta \ll 1$, the function $\cos[\overline{h} k_0 (z - z')]$ is approximated in the Δ-vicinity of the branch point $\overline{h} = 1$ by the first term of its Taylor series

$$\cos\left[\overline{h} k_0 (z - z')\right] \approx \cos[k_0 (z - z')]. \tag{C2}$$

Then the integrand in (C1) appears to be the total differential

$$G_\varphi^{BRA,(mJ)}(r_1, z - z') = c_0 \cos[k_0 (z - z')] \int\limits_{1-\Delta}^{1+\Delta} d\left\{\ln H_0\left(x^{AS}(\overline{h})\right)\right\}, \tag{C3}$$

where $c_0 = \frac{ik_0}{\pi k_0 r_1}$; $x^{AS}(\overline{h}) = \sqrt{2} k_0 r_1 \sqrt{1 - \overline{h}}$.

Notice that for obtaining (C3), the spectral function is approximated in more accurate terms than it was when expressions (19), (20) were derived. Recall that the integral in (C3) has a nonintegrable singularity at the point $\overline{h} = 1$, and it can be evaluated only in the sense of leading term. For this, put (C3) in the form

$$G_\varphi^{BRA,(mJ)}(r_1, z - z') = v \cdot p \cdot \int\limits_{1-\Delta}^{1+\Delta} d\{\ \} = \lim_{\varepsilon \to 0} \left[\int\limits_{1-\Delta}^{1-\varepsilon} d\{\ \} + \int\limits_{1+\varepsilon}^{1+\Delta} d\{\ \} \right]. \tag{C4}$$

In view of

$$\lim_{\varepsilon\to 0}\left\{\ln\left[\frac{H_0^{(2)}(x^{AS}(1-\varepsilon))}{H_0^{(2)}(x^{AS}(1+\varepsilon))}\right]\right\}=\lim_{\varepsilon\to 0}\left\{\ln\left[\frac{H_0^{(2)}(z^{AS}(\varepsilon))}{2i\pi K_0(z^{AS}(\varepsilon))}\right]\right\}=0, \tag{C5}$$

where $z^{AS}(y)=\sqrt{2}k_0r_1\sqrt{y}$, one finally obtains

$$G_{\varphi}^{BRA,(mJ)}(r_1,z-z')=c_0\ln\left[\frac{2i\pi K_0(z^{AS}(\Delta))}{H_0^{(2)}(z^{AS}(\Delta))}\right]\cos[k_0(z-z')]. \tag{C6}$$

As mentioned, the real part of the function $g_{\varphi}^{(mJ)}$ has an integrable singularity. The contribution from this singularity integration is contained in (C6). This contribution can be also obtained by the integration of asymptotic expression (19). Finally,

$$REAL\left\{G_{\varphi}^{BRA,(mJ)}(r_1,z-z')\right\}$$
$$=c_0\left\{-\frac{\pi}{2}-arctg\left[\frac{2}{\pi}\ln(\alpha\gamma/2)+0.5\ln\Delta\right]\right\}\cos[k_0(z-z')], \tag{C7}$$

where $\alpha=\sqrt{2}k_0r_1$. The results due to formula (C.7) are very close to the real part of (C.6). Yet the need to calculate the special functions is avoided. In the calculations, $\Delta=10^{-3}$.

Turn to the calculation of the function $G_z^{BRA,(mJ)}(r_1,z-z')$ given as

$$G_z^{BRA,(mJ)}(r_0,z-z')=\frac{k_0}{\pi}\int\limits_{1-\Delta}^{1+\Delta}g_z^{mJ}(r_1,\overline{h})\cos\left[\overline{h}k_0(z-z')\right]d\overline{h}. \tag{C8}$$

Notice that according to (17)–(18), only the imaginary part of $g_z^{mJ}(r_1,\overline{h})$ has a singularity at the branch point. That is a logarithmic and hence integrable singularity. Using asymptotic representations (17)–(18) and approximation (C2) gives

$$IMAG\left\{G_z^{BRA,(mJ)}(r_0,z-z')\right\}$$
$$=\cos[k_0(z-z')]\frac{k_0\Delta k_0r_1}{2\pi}[\ln\Delta-1+2\ln(\gamma\alpha/2]. \tag{C9}$$

The real part of (C8) is a smooth numerically calculated function.

APPENDIX D. PASSAGE TO THE LIMIT FROM SHEET MAGNETIC CURRENT TO RING MAGNETIC DIPOLE

Proceed to the case of current distribution as a circular dipole in (27)–(28) form. Insert (27) into (10) and integrate it to

$$\begin{aligned} H_\varphi(r_1,z) &= \int_0^L I^m_{0\varphi}\delta(z'-0)G^{mJ}_\varphi(r_1,z-z')dz' \\ &= 2\pi I^m_{0\varphi} r_1 G^{mJ}_\varphi(r_1,z-z')|_{z'=0}. \end{aligned} \tag{D1}$$

Substituting (28) into (9) yields

$$\begin{aligned} H_z(r_1,z) &= \int_0^L I^m_{0z}\delta(z'-0)G^{mJ}_z(r_1,z-z')dz' \\ &\quad + I^m_{0z}\frac{d}{dz}\int_0^L \frac{d}{dz'}\delta(z'-0)G^{m\sigma}(r_1,z-z')dz' \\ &= 2\pi r_1 I^m_{0z}\left[G^{mJ}_z(r_1,z-0) - \frac{d}{dz}\frac{d}{dz'}G^{m\sigma}(r_1,z-z')|_{z'=0}\right] \\ &= 2\pi r_1 I^m_{0z}\Phi(z-z')|_{z'=0}, \end{aligned} \tag{D2}$$

where

$$\Phi(z-z')|_{z'=0} = G^{mJ}_z(r_1,z-0) + \frac{d^2}{dz'^2}G^{m\sigma}(r_1,z-z')|_{z'=0}. \tag{D3}$$

Notice that $G^{m\sigma}_z(r_1,z-z') = (1/k_0^2)G^{mJ}_z(r_1,z-z')$. Proceeding from the appearance of $G^m_z(r_1,z-z')$ function in Fig. 6a, the just mentioned dependence when the source distance is longer than the several wavelengths can be approximated as

$$G^{mJ}_z(r_1,z-z') \approx A(z-z')e^{ik_0(z-z')}, \tag{D4}$$

where the amplitude $A(z-z')$ slowly decreases as $(z-z')$ rises. Clearly in this case,

$$\Phi(z-z') \approx -ik_0 A'_z(z-z')e^{ik_0(z-z')}. \tag{D5}$$

From (D5) it follows that as $(z-z')$ grows, function $\Phi(z-z')$ decreases faster than the function $G^{mJ}_z(r_1,z-z')$ from Fig. 6b does.

REFERENCES

1. Bertuch, Th. and C. V. Winterfeld, "Modelling of arrays of open-ended waveguide antennas," *Proc. of 2nd European Workshop on Conformal Antennas*, 65–68, Hague, April 2001.
2. Thors, B. and L. Josefsson, "The radar cross section of a conformal array antenna," *Proc. of 2nd European Workshop on Conformal Antennas*, 69–72, Hague, April 2001.
3. Schelkunoff, S. A., "Some equivalence theorems of electromagnetics and their application to radiation problems," *Bell Syst. Tech. Journ.*, Vol. 15, 92, 1936.
4. Villegas, F. J., Y. Rahmat-Sami, and D. R. Jackson, "A hybrid MoM solution of scattering from finite arrays of cylindrical cavities in a ground plane," *IEEE Transaction on Antenna and Propagation*, Vol. 51, No. 9, 2369–2380, 2003.
5. Markov, G. T. and A. F. Chaplin, "Excitation of electromagnetic waves," *Moscow: Radio & Svyaz*, 1983 (in Russian).
6. Svezhentsev, A. Ye. and G. A. E. Vandenbosch, "Spatial Green's function singularity for sheet electric current over dielectric coated cylinder," *IEEE Trans. on Antenna and Propagation*, Vol. 52, No. 2, 608–610, 2004.
7. Nosich, A. I., "Radiation condition, limiting absorption principle, and general relations in open waveguide scattering," *Journal of Electromagnetic Waves and Application*, Vol. 8, No. 3, 329–353, 1994.
8. Abramowitz, M. and I. A. Stegun, *Handbook of Mathematical Functions*, Dover, New York, 1971.
9. Prudnikov, A. P., Yu. A. Brychkov, and O. I. Marichev, *Integrals and Series. Elementary Functions*, Nauka, Moscow, 1981 (in Russian).
10. —, *Integrals and Series. Special Functions*, Nauka, Moscow, 1983 (in Russian).
11. Fikioris, J. G., "On the singular integrals in the source region of electromagnetic fields," *JEMWA*, Vol. 18, No. 11, 1505–1521, 2004.